Effect of aerosol microphysical properties on polarization of skylight: sensitivity study and measurements

Eyk Boesche, Piet Stammes, Thomas Ruhtz, Réne Preusker, and Juergen Fischer

We analyze the sensitivity of the degree of linear polarization in the Sun's principal plane as a function of aerosol microphysical parameters: the real and imaginary parts of the refractive index, the median radius and geometric standard deviation of the bimodal size distribution (both fine and coarse modes), and the relative number weight of the fine mode at a wavelength of 675 nm. We use Mie theory for single-scattering simulations and the doubling–adding method with the inclusion of polarization for multiple scattering. It is shown that the behavior of the degree of linear polarization is highly sensitive to both the small mode of the bimodal size distribution and the real part of the refractive index of aerosols, as well as to the aerosol optical thickness; whereas not all parameters influence the polarization equally. A classification of the importance of the input parameters is given. This sensitivity study is applied to an analysis of ground-based polarization measurements. For the passive remote sensing of microphysical and optical properties of aerosols, a ground-based spectral polarization measuring system was built, which aims to measure the Stokes parameters I, Q, and U in the visible (from 410 to 789 nm) and near-infrared (from 674 to 995 nm) spectral range with a spectral resolution of 7 nm in the visible and 2.4 nm in the near infrared. We compare polarization measurements taken with radiative transfer simulations under both clear- and hazy-sky conditions in an urban area (Cabauw, The Netherlands, 51.58° N, 4.56° E). Conclusions about the microphysical properties of aerosol are drawn from the comparison.

OCIS codes: 010.1110, 260.5430, 280.1310.

1. Introduction

The impact of tropospheric aerosols on the climate system is difficult to determine quantitatively. This difficulty is caused, on the one hand, by the high temporal and spatial variability of the amount, chemical composition and size of aerosols, which are difficult to determine on a global scale.[1,2] On the other hand, it is attributable to the fact that aerosol effects are taken into account rather rudimentarily in climate models.[3–5] First, the radiative forcing of climate by aerosols relates to changes in the net radiative fluxes in the atmosphere. The latter are caused by the modulation of atmospheric scattering and absorption properties attributable to anthropogenic changes in the concentration and optical properties of aerosols (the direct aerosol effect).[6] Second, cloud reflectivity is enhanced because of the increased concentration of cloud droplets associated with the increased number of condensation nuclei in polluted air (the first indirect aerosol effect).[7,8] Third, aerosols affect the microphysical properties of clouds by shifting the droplet distribution toward smaller sizes. Therefore polluted clouds are less likely to produce drizzle and less likely to rain out (the second indirect aerosol effect).[8–10] Fourth, aerosols change the concentration of radiatively effective and chemically reactive trace gases because of the heterogeneous processes that take place on their surfaces. It is already clear that the radiative forcing of aerosol particles is similar or can even exceed (with a negative sign) the radiative forcing of the anthropogenic greenhouse gases, if indirect effects are included.[4]

Microphysical parameters, such as refractive index, size distribution, and shape, are necessary as input for the calculation of optical properties, but thus far they are inadequately known for most types of aerosol. Therefore further development of adequate optical measurement methods for the determi-

When this research was performed, E. Boesche (boesche@wew.fu-berlin.de), T. Ruhtz, R. Preusker, and J. Fischer were with the Institute for Space Sciences, Free University Berlin, Carl-Heinrich-Becker-Weg 6-10, 12165 Berlin, Germany. E. Boesche is currently working with P. Stammes (stammes@knmi.nl) at the Royal Netherlands Meteorological Institute, P. O. Box 201, 2730 AE de Bilt, The Netherlands.

Received 30 March 2006; revised 7 July 2006; accepted 16 August 2006; posted 16 August 2006 (Doc. ID 69191).

0003-6935/06/348790-16$15.00/0

nation of microphysical properties of aerosol is needed.[11]

Remote sensing with ground-based passive radiation instruments can make an important contribution to fundamental studies of atmospheric aerosols. The influence of aerosols on the radiation budget at the surface can be quantified by diffuse and direct irradiance measurements with broadband pyranometers and pyrheliometers. The aerosol optical thickness can be derived from extinction measurements of direct sunlight, the aerosol size distribution from the spectral behavior of the optical thickness, and the single-scattering albedo from diffuse sky radiance measurements. Generally, this can be done only under the assumption that the other aerosol characteristics are known.[12] Sunphotometer and sky photometer are common instruments for these measurements. They are in operational use for the remote sensing of aerosols, for example, in the aerosol robotic network (AERONET).[13]

The measurements of the degree of polarization of diffuse skylight offer an additional source of information about aerosols. The consideration of polarization complements the spectral and angular radiance measurements and produces a significantly higher sensitivity to microphysical properties of aerosols than do radiance measurements.[14–16] Therefore a polarization spectrometer can be regarded as an optimal instrument for aerosol remote sensing measurements in the solar spectral range since it uses all the available information: the directional and spectral dependence of the Stokes parameters (radiance and polarization). The measurements of the angular and spectral dependence of the polarization of skylight can be used principally to estimate the refractive index, the single-scattering albedo, the columnar (or altitude-integrated) size distribution, and the aspect ratio of aerosols.[17–22] Thus far measurements and interpretations of ground-based skylight polarization are rather scarce.

Our aim is to show the sensitivity of the degree of linear polarization of skylight in the Sun's principal plane (the plane defined by the Sun and the zenith direction) to changes of the microphysical and optical properties of aerosols. This sensitivity study is applied to an interpretation of ground-based measurements of the degree of linear polarization. Ground-based measurements show that aerosol polarization comes mainly from the small spherical aerosol particles.[17] Aerosols are often assumed to be spherical. Recent studies of nonspherical tropospheric aerosols are devoted mainly to dustlike and sea saltlike tropospheric aerosols.[23–26] Considering the measurement location (Cabauw, The Netherlands) and the meteorological conditions in this area, we assume spherical aerosols for this study, thus allowing the application of Mie theory. The sensitivity study is limited to a single wavelength outside of the absorption bands. We first show the measurement results of the spectral dependence of skylight polarization, but a further investigation of the spectral information content will be part of future studies. In Section 2 the definition of relevant polarization parameters, such as the Stokes parameters and the scattering matrix, are briefly discussed. Then the sensitivity of the degree of linear polarization of skylight in the principal plane to changes in the microphysical properties of aerosols is shown for Mie single-scattering calculations (Subsections 3.A and 3.B) and multiple-scattering simulations (Subsections 3.C and 3.D). In Section 4 we outline a new ground-based measurement system of the Freie Universität Berlin integrated spectrographic system–polarization (FUBISS–POLAR). It was developed at the Institute for Space Sciences (Freie Universität Berlin) to investigate the optical properties of aerosols.[27] FUBISS–POLAR was designed to provide multiangle measurements of the polarization of diffuse skylight and measurements of the atmospheric transmission in a wide spectral range. In Section 5 we compare the FUBISS–POLAR measurements in the principal plane with the radiative transfer simulations. The comparison of radiative transfer simulations with *in situ* measurements allows us to draw conclusions regarding the aerosol refractive index, the aerosol size distribution, and the fine mode fraction of the aerosol optical thickness.

2. Definition of Polarization Parameters and Observation Geometry

A. Stokes Parameters

The state of polarization of a light beam can be defined through the components of Stokes vector $\mathbf{I}$,[28,29] by measuring the relative intensities I_α of the light beam after it has passed through polarization devices at different orientations α of their transmission axes[30]:

$$\mathbf{I} = \begin{pmatrix} I \\ Q \\ U \\ V \end{pmatrix} = \begin{pmatrix} I_{0^\circ} + I_{90^\circ} \\ I_{0^\circ} - I_{90^\circ} \\ I_{45^\circ} - I_{135^\circ} \\ I_{+} - I_{-} \end{pmatrix}, \tag{1}$$

where 0°, 45°, 90°, and 135° denote the orientations of the polarization transmission axes with respect to a reference plane, and + and − are the right- and left-handed circular polarization components. Here the reference plane can be arbitrarily chosen through the direction of propagation of the light beam. Throughout this paper we use the principal plane as the reference plane. Stokes parameter I describes the total intensity, Q and U the linear polarization, and V the circular polarization of the light beam. From the Stokes parameters the following polarization parameters can be derived[31]:

$$P = \frac{(Q^2 + U^2 + V^2)^{1/2}}{I}, \tag{2}$$

$$P_l = \frac{(Q^2 + U^2)^{1/2}}{I}, \tag{3}$$

$$P_c = \frac{V}{I}, \tag{4}$$

where P is the total degree of polarization, P_l is the degree of linear polarization, and P_c is the degree of circular polarization. Symmetry demands that $U = 0$ for skylight measurements within the principal plane. To preserve the sign of Q, the degree of linear polarization in the principal plane can be written as

$$P_s = -\frac{Q}{I}. \tag{5}$$

In the following discussion the circular component V of the Stokes vector is neglected, because numerous experiments and simulations show that V has a marginal influence on the total degree of polarization in the atmosphere.[32,33]

B. Scattering Matrix

We consider independent light scattering by an ensemble of randomly oriented particles, which has a plane of symmetry. The scattering plane contains the direction of propagation of the incident and scattered light and will serve as the reference plane. The Stokes parameters of the scattered beam for scattering angle Θ can be written as a linear transformation of the Stokes parameters of the incident beam[28,30,31]:

$$\begin{pmatrix} I_{\text{sca}} \\ Q_{\text{sca}} \\ U_{\text{sca}} \\ V_{\text{sca}} \end{pmatrix} = \begin{bmatrix} F_{11} & F_{12} & 0 & 0 \\ F_{12} & F_{22} & 0 & 0 \\ 0 & 0 & F_{33} & F_{34} \\ 0 & 0 & -F_{34} & F_{44} \end{bmatrix} \begin{pmatrix} I_{\text{in}} \\ Q_{\text{in}} \\ U_{\text{in}} \\ V_{\text{in}} \end{pmatrix}, \tag{6}$$

where the subscripts "sca" and "in" stand for scattered and incoming beams. The matrix $\mathbf{F}$, with elements F_{ij}, is called the scattering matrix, and its elements are functions of the scattering angle. Owing to the constraints on the ensemble of particles, the scattering matrix has only six independent elements. The scattering matrix depends on the refractive index, the size distribution, and the shape of the scattering particles and contains all the polarizing properties of the ensemble of randomly oriented particles.

For spherical particles, the scattering matrix can be calculated using Mie theory. If the incident light is nonpolarized, the first column of the scattering matrix suffices to determine the intensity and state of polarization of the light scattered once. For accurate multiple-scattering calculations, however, the complete scattering matrix is necessary because nonpolarized light becomes polarized after being scattered. Function F_{11} is called the phase function and is normalized such that

$$\frac{1}{2}\int_0^1 F_{11}(\Theta)\sin\Theta d\Theta = 1. \tag{7}$$

For nonpolarized incident light, F_{11} is proportional to the scattered intensity as a function of the scattering angle. The ratio $-F_{12}/F_{11}$ represents the degree of linear polarization if the incoming light is nonpolarized [see Eq. (5)]. Furthermore, we must have $|F_{ij}/F_{11}| \leq 1$, and for spheres the relations $F_{11} = F_{22}$ and $F_{33} = F_{44}$ hold.[34]

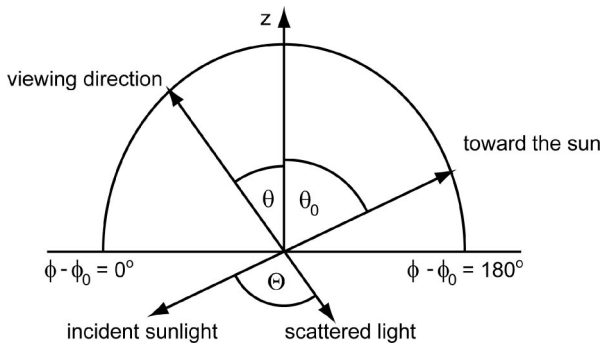

Fig. 1. Scattering geometry in the principal plane. The viewing direction and the solar direction are, together with the local vertical, in one plane. Θ is the scattering angle.

C. Geometric Characteristics for the Atmosphere

The direction of radiation at an arbitrary point within the atmosphere is specified by zenith angle θ and azimuth angle ϕ (see Fig. 1). The direction of incident sunlight is specified by θ_0 and ϕ_0. Zenith angle θ is measured from the positive z direction, i.e., the local vertical. Azimuth angle ϕ is measured clockwise when looking in the positive z direction. The zero direction of the azimuth is arbitrary; thus only differences in azimuth $\phi - \phi_0$ are important. In the principal plane the scattering angle Θ between the incident light and the scattered light (see Fig. 1) is given as follows: for $\phi - \phi_0 = 0°$, the scattering angle is $\Theta = |\theta_0 - \theta|$; for $\phi - \phi_0 = 180°$, $\Theta = \theta_0 + \theta$. The angular ranges are as follows: $0° \leq \theta, \theta_0 \leq 90°$, $0° \leq \phi \leq 360°$, and $0° \leq \Theta \leq 180°$.

3. Simulations of the Degree of Linear Polarization of Skylight

Here we discuss the sensitivity of the degree of linear polarization to changes of aerosol microphysical and optical properties. This sensitivity is studied here using Mie calculations (Subsections 3.A and 3.B) and multiple-scattering simulations (Subsections 3.C and 3.D). From the Mie single-scattering calculations of the degree of linear polarization as a function of scattering angle $P_s(\Theta)$ we further derive the single-scattering albedo ω and the scattering matrix $\mathbf{F}(\Theta)$. These values, taken from selected Mie calculations, serve as input for the multiple-scattering simulations of the degree of linear polarization as a function of the viewing zenith angle $P_s(\theta)$. For the simulations we use a standard set of aerosol input parameters (see Tables 1 and 2) and change one of the parameters in a given range, and the others remain unchanged.

A. Mie Calculation Input Parameters

The degree of linear polarization of single scattering by spherical particles is computed by using Mie scattering theory.[35] The input parameters required for

Table 1. Mie Simulation Input Parameters[a]

Parameter	Symbol	Standard Value (Cabauw, The Netherlands)	Range	Greenbelt (USA)	Paris (France)
Wavelength	λ (μm)	0.675	Constant	0.675	0.675
Real part of the refractive index	m_r	1.400	1.330–1.600	1.410	1.400
Imaginary part of the refractive index	m_i	0.007	0.000–0.020	0.003	0.009
Median radius of the fine mode	r_f (μm)	0.080	0.010–0.110	0.081	0.067
Median radius of the coarse mode	r_c (μm)	0.425	0.150–0.650	0.565	0.428
Standard deviation of the fine mode	σ_f	1.400	1.200–2.200	1.460	1.537
Standard deviation of the coarse mode	σ_c	2.200	1.500–2.500	2.120	2.203
Weighting factor of the fine mode	w	0.9995	0.998–1.000	0.9995	0.9995

[a]The Cabauw values are used as standard input for the Mie simulations. The fourth column gives the range in which the values are varied for the sensitivity study. For comparison purposes the fifth and sixth columns give the average values as measured by AERONET in urban locations (Greenbelt and Paris).[11]

Mie calculations include (see also Table 1): wavelength λ of the incident light, the real and imaginary parts of aerosol refractive index m, and the aerosol size distribution. The wavelength was chosen to be 675 nm, where only ozone absorption in the Chappuis band has to be taken into account, and remains constant throughout the sensitivity study. As size distribution, a bimodal lognormal distribution was chosen, given by

$$n_N(r) = \frac{dN}{dr} = w\,\frac{N_f}{\sqrt{2\pi}\ln(\sigma_f)}\,\frac{1}{r}\exp\left\{-\frac{1}{2}\left[\frac{\ln(r)-\ln(r_f)}{\ln(\sigma_f)}\right]^2\right\} + (1-w)\frac{N_c}{\sqrt{2\pi}\ln(\sigma_c)} \times \frac{1}{r}\exp\left\{-\frac{1}{2}\left[\frac{\ln(r)-\ln(r_c)}{\ln(\sigma_c)}\right]^2\right\}, \quad (8)$$

where $n_N(r)$ is the number distribution ($\mu m^{-1} cm^{-3}$), $N_{f,c}$ are the total aerosol number concentrations for the fine and coarse modes, $r_{f,c}$ are the fine and coarse mode number median radii, $\sigma_{f,c}$ are the fine and coarse mode geometric standard deviations of the distribution,[36] and w is the weighting factor of the fine mode. The typical values for weighting factor w are in the range of 0.9992–0.9998.[37] It is sometimes convenient for comparison between size distributions to express the size parameters of different distributions in terms of two common parameters, the effective radius and the effective variance. For each mode the effective radius r_{eff}, or area weighted mean radius, can be used as larger particles tend to be more efficient scatterers:

$$r_{\text{eff},i} = r_i(1 + v_{\text{eff},i})^{2.5}, \qquad i = f,\ c, \quad (9)$$

where i represents fine and coarse mode values [see also Eq. (8)]. Similarly for the standard deviation of a distribution, the effective variance v_{eff} can be used:

$$v_{\text{eff},i} = \exp[\ln(\sigma_i)^2] - 1, \qquad i = f,\ c. \quad (10)$$

An advantage of the lognormal distribution is that the standard deviations for the number, surface, and volume distributions are identical, and therefore the surface median radius r_S and the volume median radius r_V can be written in terms of the number median radius r_N and standard deviation σ_N as follows[36]:

$$\ln(r_{S,i}) = \ln(r_{N,i}) + 2\ln^2(\sigma_{N,i}), \quad i = f,\ c, \quad (11)$$

$$\ln(r_{V,i}) = \ln(r_{N,i}) + 3\ln^2(\sigma_{N,i}), \quad i = f,\ c. \quad (12)$$

To have realistic standard aerosol input parameters for the single- and multiple-scattering calcula-

Table 2. Input Parameters for the DAK Multiple Scattering Simulations[a]

DAK Input Parameter	Symbol	Standard Value (Cabauw, The Netherlands)	Range
Wavelength	λ (μm)	0.675	Constant
Surface albedo	A	0.10	0.05–0.20
Atmospheric profile		Mid-latitude Summer, AFGL (1986)	—
Number of atmospheric layers	N	32	Constant
Aerosol altitude	h (km)	0–1	0–16
Mie input parameters		See Table 1	—
Aerosol optical thickness	τ_{aer}	0.065	0.045–0.400

[a]The third column gives the standard Cabauw case values for 11 October 2004. The fourth column gives the range in which the parameters are varied in the sensitivity study.

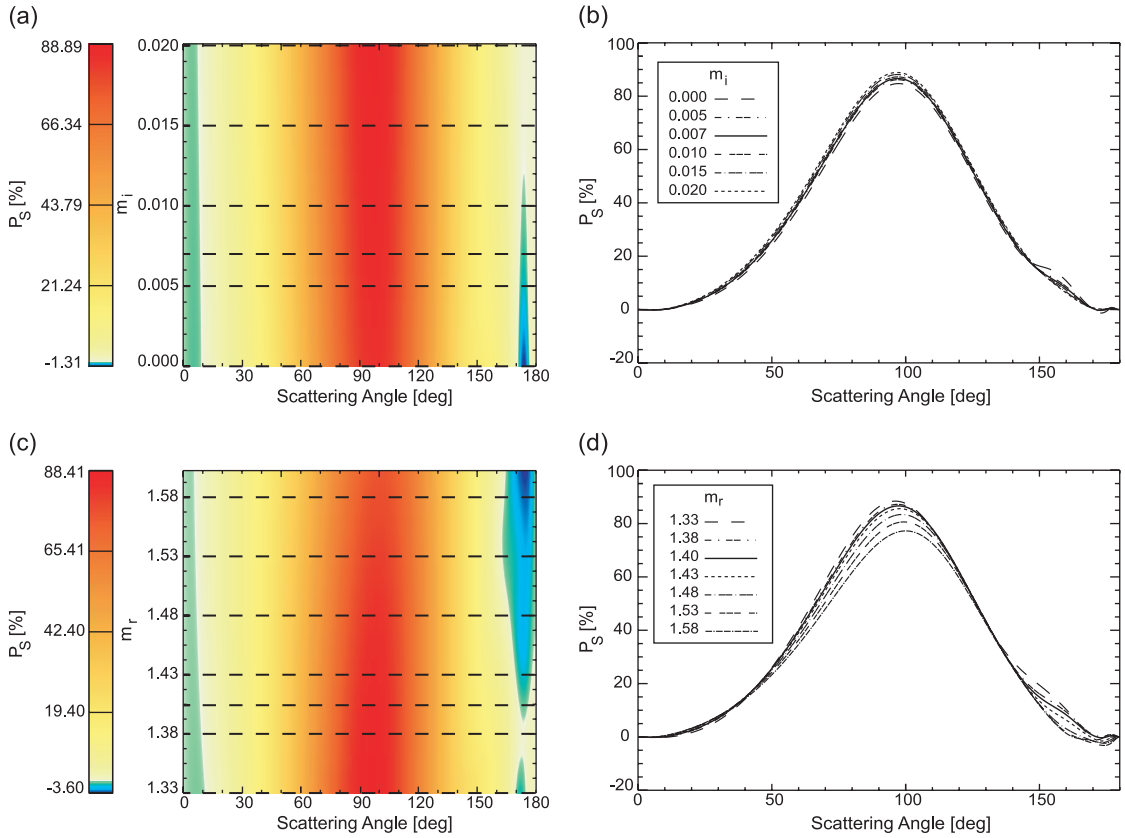

Fig. 2. Mie simulations of the degree of linear polarization P_s at $\lambda = 675$ nm as a function of the scattering angle and varied aerosol parameter. The Cabauw case was used as standard input and one parameter was varied, and the others remain unchanged (see Table 1). The varied parameters are (a), (b), the imaginary part of the refractive index and (c), (d), the real part of the refractive index. The left column shows the degree of linear polarization versus the varied input parameter and scattering angle. The color bar goes from red to yellow ($P_s > 0$) to white ($P_s = 0$) and from green to blue ($P_s < 0$). In the right column, the corresponding *xy* plots show slice planes of the degree of linear polarization versus the scattering angle. The slice planes are indicated in the colored figures by dashed lines. For comparison, the Cabauw case is indicated by a solid black curve in the slice plane figures.

tions, we constructed a precalculated lookup table, which was based on AERONET climatology data including the variability for several sites.[38] We compared measurements of the degree of linear polarization in the principal plane, taken on 11 October 2004 in Cabauw, The Netherlands (see Section 5) and the lookup table results. The parameters of the best fit, subsequently referred to as the Cabauw case (see Table 1), were taken as the standard input for the Mie sensitivity study. The range of the real and imaginary parts of refractive index m, as well as the number median radii $r_{f,c}$ and the geometric standard deviations $\sigma_{f,c}$ of the aerosol size distribution chosen for the sensitivity study, comprise a wide range of tropospheric aerosol properties.[38,39] The same refractive index has been assumed for the fine and coarse mode particles of the aerosol size distribution.

B. Mie Single-Scattering Polarization Results

The focus of the single-scattering sensitivity study of the degree of linear polarization as a function of scattering angle $P_s(\Theta)$ turns on the following four criteria: the sensitivity of the polarization in the forward-scattering direction ($0° < \Theta < 90°$), the sensitivity of the polarization in the backscattering direction ($90° < \Theta < 180°$), the sensitivity of the maximum degree of linear polarization, and the sensitivity of its position.

The color contour diagrams in the left panels of Figs. 2–4 present the complete picture of the behavior of $P_s(\Theta)$ as a function of each aerosol microphysical parameter. The corresponding *xy* plots in the right panels show the slice planes of $P_s(\Theta)$ for certain values of the varied input parameters. The values are indicated in the contour diagrams by dashed horizontal lines. For comparison of the $P_s(\Theta)$ curves, the standard Cabauw case is indicated by solid black curves in the right panels.

For $P_s(\Theta)$ in the forward-scattering direction, the strongest influence is found for changes of the median radius, the standard deviation, and the weighting factor of the fine mode [see Figs. 3(a), 3(b), 4(a), 4(b), 4(e), and 4(f)]. The variations of the real part of the refractive index and median radius of the coarse mode have a minor influence [see Figs. 2(c), 2(d), 3(c), and 3(d)], while variations of the imaginary part of the refractive index and the standard deviation of the coarse mode have an insignificant influence [see Figs.

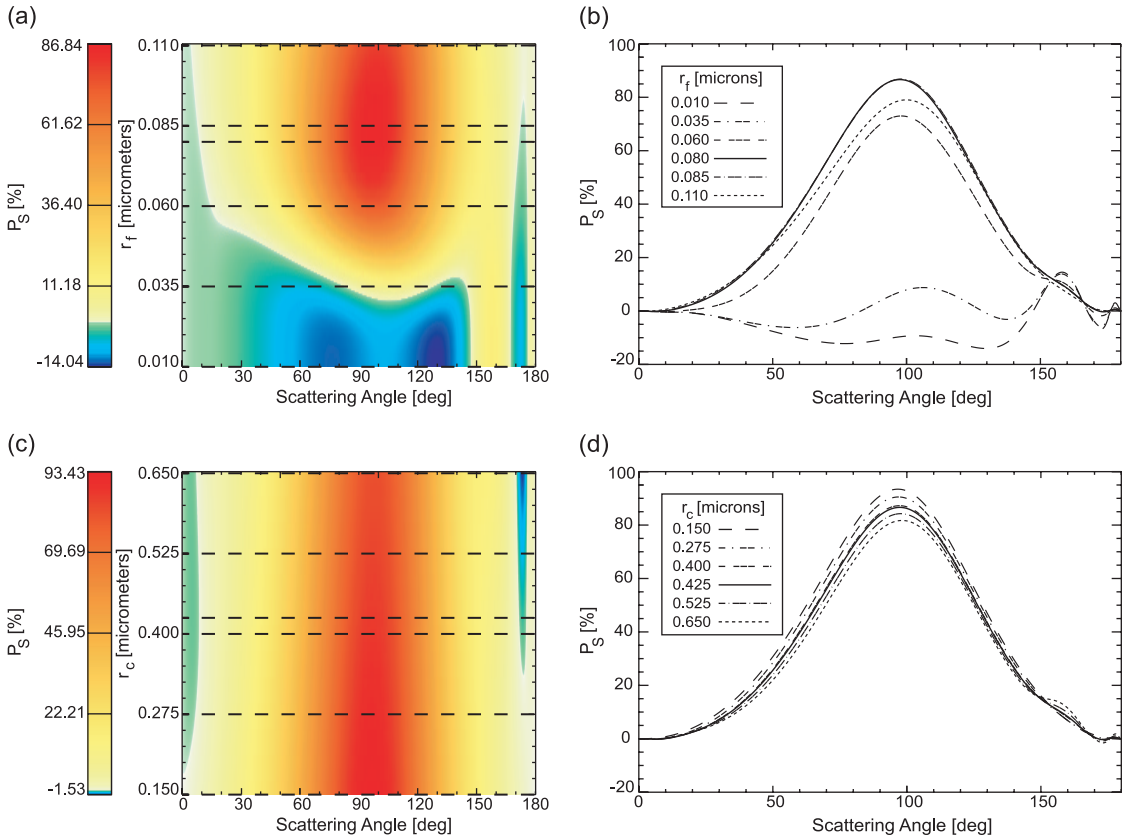

Fig. 3. Same as in Fig. 1, but for the median radius of (a), (b), the fine mode and (c), (d), the coarse mode.

2(a), 2(b), 4(c), and 4(d)]. For the maximum degree of linear polarization, the influence is strongest for the fine modes of the median radius, the standard deviation, and the weighting factor [see Figs. 3(a), 3(b), 4(a), 4(b), 4(e), and 4(f)]. The real part of the refractive index and the median radius of the coarse mode have a weaker influence [see Figs. 2(c), 2(d), 3(c), and 3(d)], while the imaginary part of the refractive index and the standard deviation of the coarse mode have an insignificant influence on the maximum [Figs. 2(a), 2(b), 4(c), 4(d)]. For the position of the maximum degree of linear polarization, the strongest influence can be found by varying the real part of the refractive index [see Figs. 2(c) and 2(d)]. For $P_s(\Theta)$ in the backscattering direction, the strongest influence is found for changes in the fine modes of the median radius, the standard deviation, and the weighting factor [see Figs. 3(a), 3(b), 4(a), 4(b), 4(e), and 4(f)]. Changes in the other Mie input parameters have a minor or insignificant influence on the degree of polarization in the backscattering direction.

C. Radiative Transfer Model and Input Parameters

The DAK [doubling–adding Royal Netherlands Meteorological Institute (KNMI)] model is designed for the line-by-line calculations of radiance, polarization, and irradiance at the top of the atmosphere (TOA) inside the atmosphere. It consists of an atmospheric shell around a monochromatic multiple scattering kernel, based on the polarized doubling–adding method.[40,41] The calculation of the polarized internal radiation field of the atmosphere is described by de Haan.[40] The atmosphere may consist of an arbitrary number of plane-parallel layers, each of which can have Rayleigh scattering, gas absorption, aerosol and/or cloud particle scattering, and absorption. Polarization is fully taken into account. The atmospheric shell describes the optical parameters of each layer: optical thickness, single-scattering albedo, and scattering matrix.[40] To be used in DAK, the scattering matrix must be expanded in so-called generalized spherical functions, which is done by the Mie scattering code.[35] Because of the strong forward peak of the aerosol phase function (which can amount to 3 orders of magnitude in F_{11} between 0° and 10°), the number of expansion coefficients needed for an accurate representation of the phase function is too high for practical purposes (computation time). For this reason, a delta approximation is used before the expansion is started for all the phase functions (see Appendix A).

The degree of linear polarization is computed by using multiple-scattering simulations (DAK). The input parameters required for the DAK simulations include (see Table 2): a mid-latitude summer atmospheric profile, aerosol altitude h, aerosol optical thickness τ_{aer}, surface albedo A, Mie scattering matrices, and single-scattering albedo ω. The aerosol

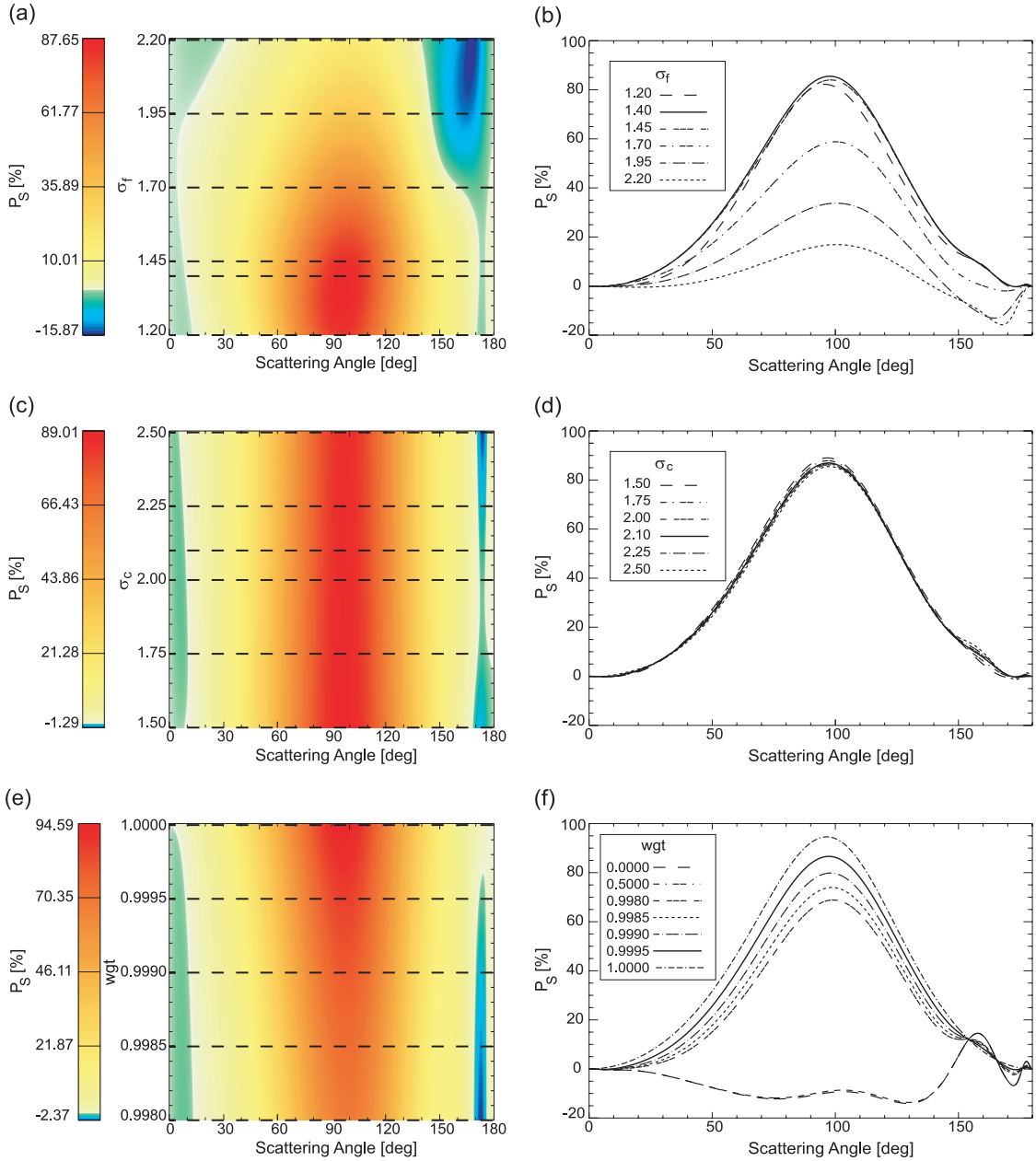

Fig. 4. Same as in Fig. 1, but for the standard deviation of (a), (b), the fine mode; the standard deviation of (c), (d), the coarse mode; (e), (f), the weighting factor of the fine mode.

was placed in the lowest kilometer of the atmosphere. The ozone absorption in the Chappuis band was included in the calculations. The standard value of the aerosol optical thickness at 675 nm was chosen according to sunphotometer measurements made on a clear day (11 October 2004) in Cabauw, The Netherlands. The surface albedo of the surrounding grassland was chosen according to the database of Koelemeijer *et al.*[42] for October at a wavelength of 675 nm. The Mie-scattering matrices, selected from the sensitivity study in Subsection 3.B and shown in the right panels of Figs. 2–4, served as aerosol input parameters for the DAK simulations. The Cabauw case aerosol was used as the standard aerosol model (Table 1). For a comparison of the different figures of the sensitivity study, the Cabauw case is indicated by a solid black curve in Figs. 5 and 6.

D. Multiple-Scattering Simulations of Polarization of Skylight

The focus for the multiple scattering simulations turns on the same four aspects of the sensitivity of skylight polarization on aerosol microphysical parameters as in Subsection 3.B: the sensitivity of the polarization in the forward-scattering direction, the sensitivity of the polarization in the backscattering direction, the sensitivity of the maximum polarization, and the sensitivity of the position of the maximum degree of linear polarization. The standard input parameters for this sensi-

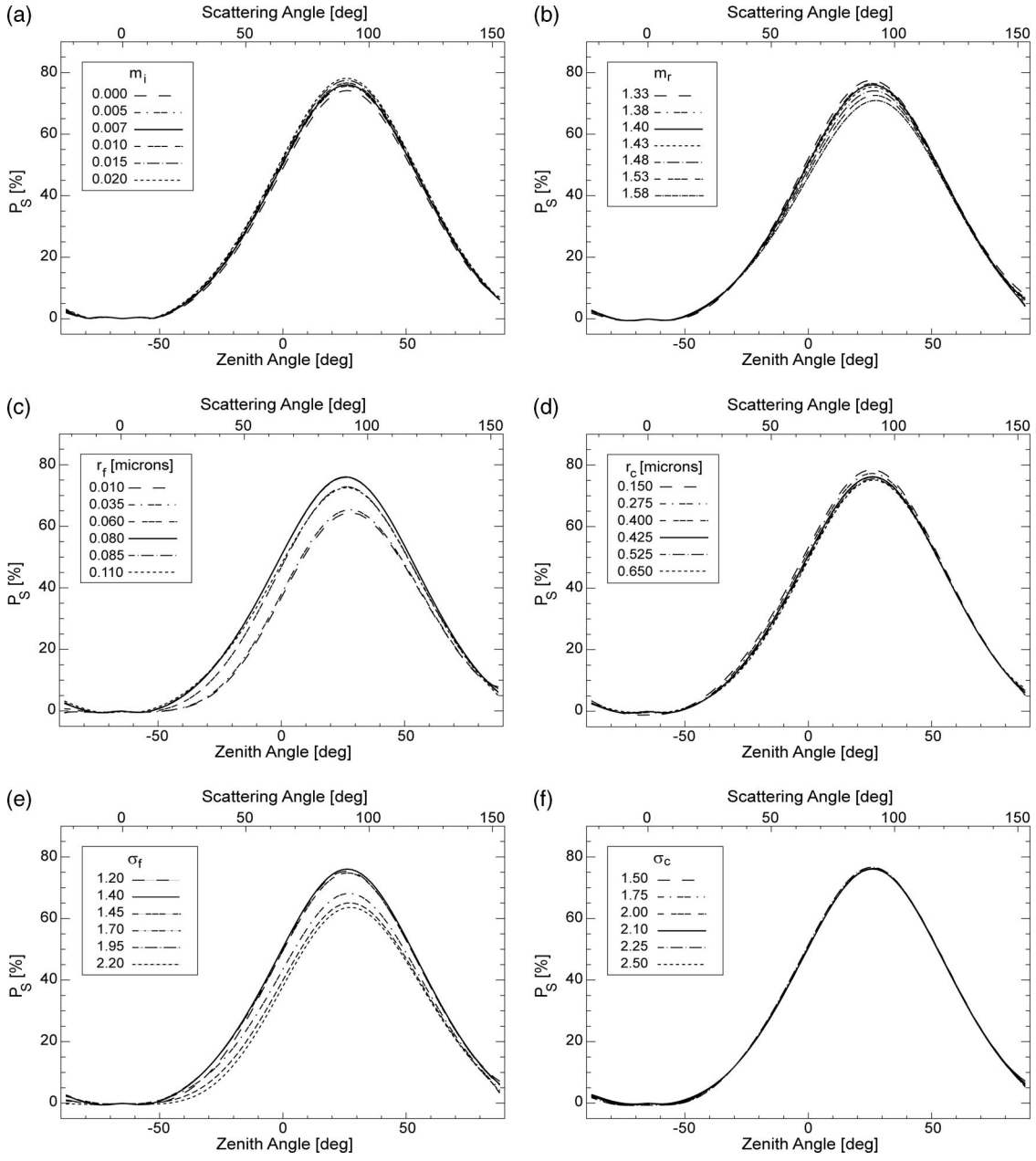

Fig. 5. Multiple scattering simulations, using DAK, of the degree of linear polarization P_s at $\lambda = 675$ nm as a function of the zenith and scattering angles in the principal plane at a solar zenith angle of $\theta_0 = 65°$. Negative zenith angles refer to $\phi - \phi_0 = 0°$, and positive zenith angles to $\phi - \phi_0 = 180°$ (see Subsection 2.C). The Cabauw case (solid curve) was used as standard input, and one parameter was varied, while the others remain unchanged (see Tables 1 and 2). The varied parameters are (a) the imaginary part of the refractive index, (b) the real part of the refractive index, (c) the median radius of the fine mode, (d) the median radius of the coarse mode, (e) the standard deviation of the fine mode, (f) the standard deviation of the coarse mode.

tivity study refer to very clear-sky conditions (the Cabauw case).

For $P_s(\theta)$ in the forward-scattering direction, the strongest influence is found for variations of the fine mode median radius and the fine mode standard deviation [see Figs. 5(c) and 5(e)]. The influence of the real part of the refractive index, the weighting factor of the fine mode, and the aerosol optical thickness are less significant [see Figs. 5(b), 6(a), and 6(c)]. The other input parameters have a minor or insignificant influence on the polarization in the forward-scattering direction. The maximum degree of linear polarization is strongly influenced by nearly all the input parameters. The only exceptions are the coarse mode radius, the coarse mode standard deviation, the imaginary part of the refractive index, and the aerosol altitude, which have a minor or insignificant influence [see Figs. 5(a), 5(d), 5(f), and 6(b)]. For the position of the maximum degree of linear polarization, influences can be found for the real part of the refractive index, the fine mode median radius, and the standard deviation [see Figs. 5(b), 5(c), and 5(e)]. $P_s(\theta)$ in the backscattering direc-

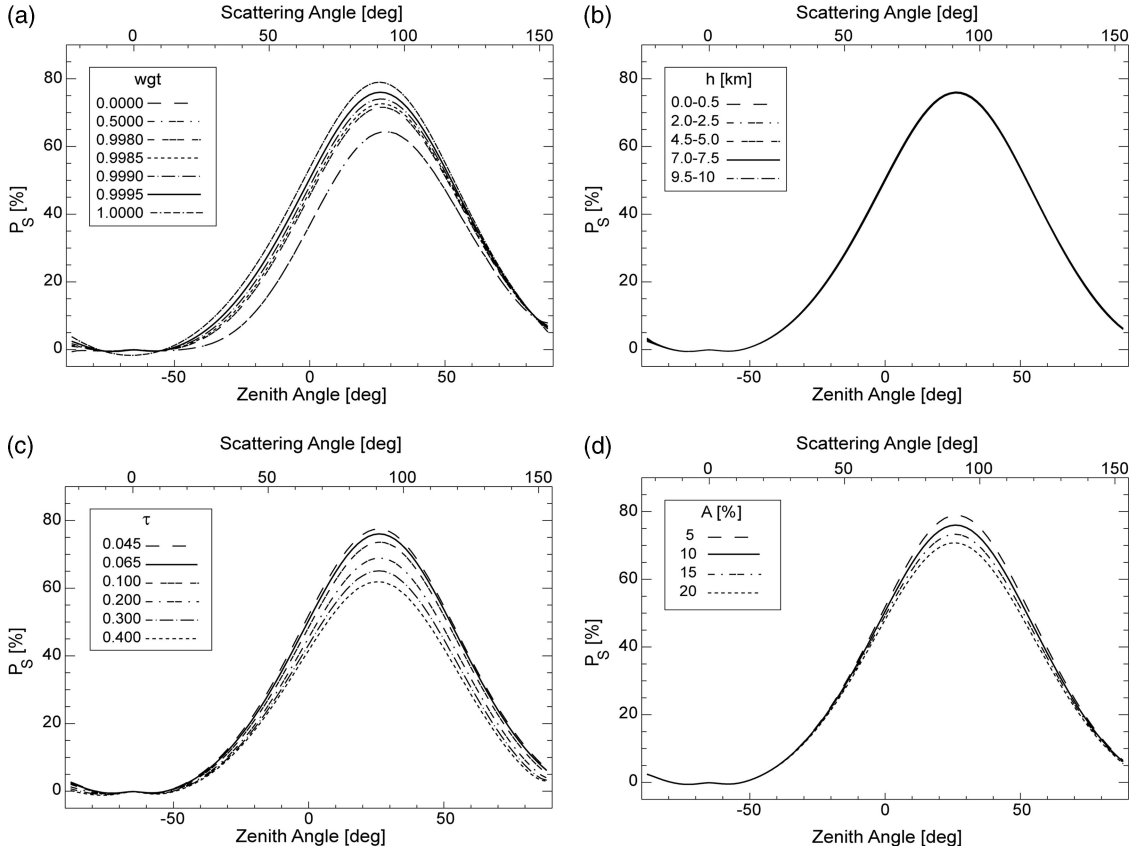

Fig. 6. Same as in Fig. 5, but for the weighting factor of (a) the fine mode, (b) the aerosol altitude, (c) the aerosol optical thickness, (d) the surface albedo.

tion is influenced mainly by the fine mode median radius, the standard deviation of the fine mode, and by the optical thickness [see Figs. 5(c), 5(e), and 6(c)]. The variations of the weighting factor and surface albedo have a weaker effect [see Figs. 6(a) and 6(d)]. The other parameters have an insignificant influence on the degree of linear polarization in the backscattering direction.

We also studied the sensitivity of $P_s(\theta)$ for very hazy-sky conditions. For hazy-sky aerosol parameters, derived on 8 May 2003 (Table 3), we found an increase in the sensitivity $P_s(\theta)$ for the real and imaginary parts of the refractive index, whereas the sensitivity of $P_s(\theta)$ because of the changes in the weighting factor decreased strongly as compared with the clear-sky case. The strong influence of the fine mode median radius and the fine mode standard deviation remained, as did the influence of the aerosol optical thickness on $P_s(\theta)$.

The influence of all the input parameters on the degree of linear polarization of skylight for both sky conditions (very clear and hazy) is summarized in Table 4. For classification of the input parameters we examined the impact of a relative parameter change of 10% based on the parameter ranges (see Tables 1 and 2) compared to the Cabauw case. We classified parameters with an absolute effect on the maximum degree of linear polarization $\Delta P_{s,\max}$ as follows:

- $\Delta P_{s,\max} \geq 1\% \equiv ++$, very significant,
- $0.5 \leq \Delta P_{s,\max} < 1\% \equiv +$, significant,
- $0.1 \leq \Delta P_{s,\max} < 0.5\% \equiv -$, minor,
- $\Delta P_{s,\max} < 0.1\% \equiv --$, insignificant.

For the position of maximum polarization $\Delta\Theta_{P,\max}$ we used the following criteria: $\Delta\Theta_{P,\max} \geq 0.5^\circ \equiv ++$, $0.25^\circ \leq \Delta\Theta_{P,\max} < 0.5^\circ \equiv +$, $0.1^\circ \leq \Delta\Theta_{P,\max} < 0.25^\circ \equiv -$, and $\Delta\Theta_{P,\max} < 0.1^\circ \equiv --$. For classification of input parameters and their effect on polarization in the forward- and backscattering directions, we followed a more qualitative approach by comparing the relative impact of all the input parameters. The results of this sensitivity study are used for the interpretation of measurements of skylight polarization in Section 5. The instrumental setup is described first in Section 4.

4. Instrument Description

Here we give an overview of the polarization spectrometer FUBISS–POLAR (see Fig. 7 and Table 5).[27,43] FUBISS–POLAR is designed to measure the degree of linear polarization of scattered skylight with a medium spectral resolution in the visible spectral range (400–700 nm) and with a high spectral resolution in the near infrared (700–900 nm), including the O_2A band. Its optical front end consists of two identical entrance units. One entrance unit is linked via fiber optics with broadband spectrometers (with a

Table 3. Summary of the Aerosol Model Parameters for Clear (11 October 2004) and Hazy (8 May 2003) Sky Conditions

Parameter	Symbol	Cabauw Standard Case	Best Fit for 11 October 2004	Best Fit for 8 May 2003
Aerosol microphysical parameters (Mie)				
Wavelength	λ (μm)	0.675	0.675	0.675
Imaginary part of the refractive index	m_i	0.007	0.0007	0.0000
Real part of the refractive index	m_r	1.400	1.400	1.380
Median radius of the fine mode	r_f (μm)	0.080	0.080	0.120
Median radius of the coarse mode	r_c (μm)	0.425	0.425	0.700
Standard deviation of the fine mode	σ_f	1.400	1.300	1.950
Standard deviation of the coarse mode	σ_c	2.200	2.200	2.200
Weighting factor of the fine mode	w	0.9995	0.9996	0.9992
Average volume	V	0.0055	0.0069	0.0725
Average volume fine mode	V_f	0.0036	0.0029	0.0538
Macrophysical parameters (DAK)				
Aerosol altitude	h (km)	1	1	1
Aerosol optical thickness	τ_{aer}	0.065	0.065	0.390
Surface albedo	A	0.10	0.10	0.15
Mean deviation of the degree of polarization (fit measurement)	(%)	1.49	0.30	−0.811
RMSE of the degree of polarization (fit measurement)	(%)	1.35	0.76	0.91
Single-scattering albedo	ω	0.887	0.977	1.000
Fine mode fraction of τ_{aer}	(%)	70	51	17

spectral resolution of 7 nm) for the visible spectral range, and the other with high spectral resolution spectrometers (with spectral resolution of 2.4 nm) for the near-infrared spectral range. Each entrance optical unit is equipped with four entrance tubes. Each tube contains a Glan–Thompson polarization prism with a different orientation of its polarization axis (0°, 45°, 90°, and 135°) and baffles for stray light suppression. The design allows arbitrary positioning of the entrance optics within the upper hemisphere. The possible measurement geometries are the principal plane and the almucantar (see also Fig. 1). The measured intensity I_α at a polarization prism axis orientation angle α is related to Stokes parameters I, Q, and U as follows:

$$I_\alpha = \frac{1}{2}[I + Q\cos 2(\gamma + \alpha) + U \sin 2(\gamma + \alpha)], \quad (13)$$

where γ is the initial position of the polarization prism axes in the reference plane, which can be set to zero without loss of generality.

Table 4. Classification of the Importance of the DAK and Mie Input Parameters[a]

Parameters		Forward Polarization		Maximum Polarization		Position of Maximum		Backward Polarization	
		Clear	Hazy	Clear	Hazy	Clear	Hazy	Clear	Hazy
Microphysical aerosol parameters (Mie)									
Imaginary part of the refractive index	m_i	−	+	−	+	−−	−−	−−	+
Real part of the refractive index	m_r	+	++	+	++	−	+	−−	++
Median radius of the fine mode	r_f	++	++	++	++	−−	−	+	+
Median radius of the coarse mode	r_c	−	−−	−	−−	−	−−	−−	−−
Standard deviation of the fine mode	σ_f	++	++	++	++	+	++	+	+
Standard deviation of the coarse mode	σ_c	−−	−−	−−	−−	−−	−−	−−	−−
Weighting factor of the fine mode	w	+	−−	+	−−	−	−−	−	−−
Macrophysical parameters (DAK)									
Aerosol altitude	h	−−	−−	−−	−−	−−	−−	−−	−−
Aerosol optical thickness	τ_{aer}	+	++	++	++	−−	−−	++	++
Surface albedo	A	−−	−−	+	−	−−	−−	−	−

[a]The classification is for multiple scattering simulations (column 1) and their effects on the degree of linear polarization in the forward-scattering direction (column 2), the maximum polarization (column 3), the position of the maximum (column 4), and the polarization in the backscattering direction (column 5). Two sky cases are considered: clear sky (11 October 2004, Table 3) and hazy sky (8 May 2003, Table 3). Classification of the effects is as follows: very significant (++), significant (+), minor (−), and insignificant (−−) (see Subsection 3.D).

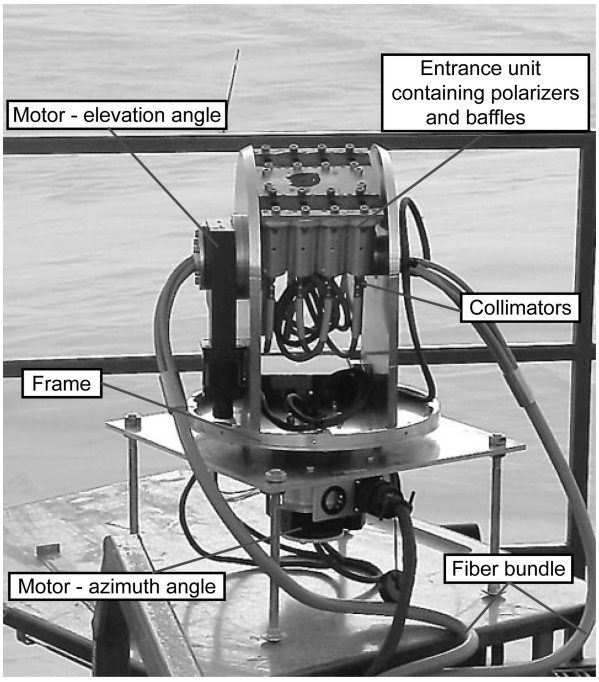

Fig. 7. Setup of the polarization spectrometer FUBISS–POLAR. The instrument measures Stokes parameters I, Q, and U simultaneously at each scan angle.

To calculate Stokes parameters I, Q, and U, only three intensity measurements at different polarization prism axis angles are needed. However, a fourth measurement leads to an overdetermined system of equations and to a redundancy that allows a rough error estimation.[43] The axis orientations of the FUBISS–POLAR polarization prisms are 0°, 45°, 90°, and 135°. The optical front end also comprises a four-quadrant diode to track the Sun position. This information is used to correct the alignment of the entrance optics by motors that are mounted at the frame construction. Measurements during a sky scan can be done continuously or at defined directions. FUBISS–POLAR is able to scan the principal plane or the almucantar within minutes, depending on the integration time, so that the Sun's relative position changes marginally. Since FUBISS–POLAR measures the intensities $I_{0°}$, $I_{45°}$, $I_{90°}$, and $I_{135°}$ simultaneously, it can be used for measurements of temporally varying objects. The system works autonomously, i.e., it takes the variation of the Sun's position into account. These are important advantages compared with other polarization measurement systems.[44–47] From the investigation of the random errors (signal-to-noise ratio and calibration standard stability) and the systematic errors (pointing error, fiber optics error, instrument polarization, and polarization prism accuracy)[27,43] the absolute polarimetric accuracy is estimated to be 1% and the alignment error is estimated to be 0.5°.

Table 5. Technical Data of the FUBISS–POLAR Polarization Spectrometer

Characteristics	MCS–VISNIR[a] (Zeiss)	MMS–UVVIS[b] (Zeiss)
Number of spectrometers	4	4
Number of channels	512	256
Spectral range	674–1082 nm	248–790 nm
Signal-to-noise ratio	<8100	<10000
Wavelength accuracy (absolute)	<0.6 nm	0.3 nm
Resolution (FWHM)	2.4 nm	7 nm
Field of view	4°	
Sun tracker alignment accuracy	0.07°	
Measurement geometries	Principal plane, almucantar, zenith	

[a]MCS, multichannel spectrometer; VISNIR, visible near infrared.
[b]MMS, monolithic miniature spectrometer; UVVIS, ultraviolet visible.

5. Comparison of Measurements and Model Results

Here we compare the multiangle measurements of the degree of polarization of skylight with the radiative transfer simulations. Conclusions about the aerosol refractive index, the aerosol size distribution, and the fine mode fraction of the aerosol optical thickness are drawn from the comparison. As an indication of whether the derived aerosol size parameters were oriented in the right direction, we looked at the spectral behavior of the maximum degree of polarization (see Fig. 8) and the Angström coefficient α derived from the sunphotometer measurements and the Mie simulations. The Angström coefficient is the exponent of a power-law fit to the aerosol optical thickness: $\tau_{aer}(\lambda) \propto \lambda^{-\alpha}$, or equivalently to the Mie extinction cross section. Using only two wavelengths for determining α, we have $\alpha = \{\ln[\tau_{aer}(\lambda_1)] - \ln[\tau_{aer}(\lambda_2)]\}/[\ln(\lambda_2) - \ln(\lambda_1)]$. The smaller the Angström coefficient, the bigger the aerosol particle size.

The measurements were taken with the polarization spectrometer FUBISS–POLAR described in Section 4. The measurement site was located at Cabauw, The

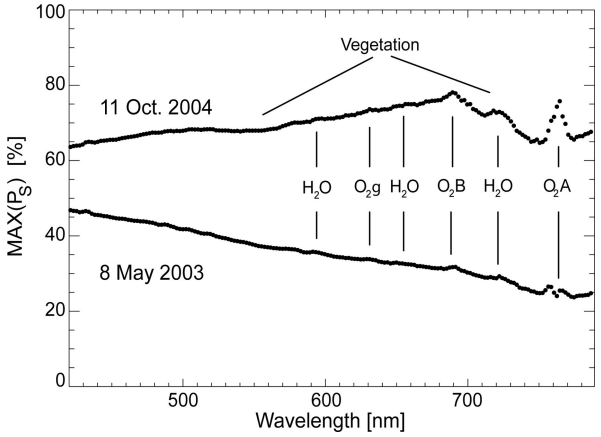

Fig. 8. Maximum degree of polarization as a function of wavelength as measured at Cabauw, The Netherlands on 11 October 2004 at a solar zenith angle of $\theta_0 = 65°$ and on 8 May 2003 at a solar zenith angle of $\theta_0 = 71°$.

Table 6. Meteorological Conditions During the Measurements

Date and Time	Solar Zenith Angle (deg.)	Temperature [°C]	Pressure (hPa)	Relative Humidity (%)	Wind Speed (m/s)
8 May 2003 06:15 UTC	70.81	10.9	1017.8	100	4.2
11 October 2004 09:55 UTC	65.02	9.5	1021.2	81	6.9

Netherlands (51.58° N, 4.56° E). The measurements of polarization in the principal plane were taken under cloudless conditions on 8 May 2003 and 11 October 2004.

The measurements on 8 May 2003 were taken at 06:15 UTC at a solar zenith angle of $\theta_0 = 71°$ in 0.4° steps of viewing zenith angle θ. The integration time was 410 ms, and one sky scan took less than 4 min. The aerosol optical thickness was $\tau_{aer} = 0.39$ at 675 nm, as measured in Cabauw by the SPUV sunphotometer (Yankee Environmental Systems, Turners Falls, Massachusetts).[48] During the measurements the sky was cloudless, but it remained hazy the whole morning. At approximately noon, convective clouds started to develop. The surface albedo A of Cabauw in May at 675 nm was assumed to be 0.10.[42] The measurements on 11 October 2004 were taken at 09:55 UTC at a solar zenith angle of $\theta_0 = 65°$ in 2.5° steps of viewing zenith angle θ. The integration time was 500 ms, and one sky scan took less than 1 min. The aerosol optical thickness was $\tau_{aer} = 0.065$ at $\lambda = 675$ nm. The whole day was very clear and cloudless. As a comparison, the multiyear average aerosol optical thickness at $\lambda = 675$ nm in Cabauw was approximately 0.15. The surface albedo A of Cabauw in October at 675 nm was assumed to be 0.15.[42] The most important meteorological conditions for the two measurement days are combined in Table 6.

The skylight polarization measurements $P_s(\theta)$ at 675 nm for both days are shown in Figs. 9(a), 9(b), and 10(a). The observations are shown with their absolute error bars, i.e., 1% for polarization and 0.5° for the viewing direction.

A. Clear-Sky Comparison for 11 October 2004

A lookup table of the calculated degree of skylight polarization (see also Section 3) for different aerosol microphysical properties was searched automatically to find the best fit to the data. The aerosol model parameters found from this lookup table were then used as a starting point for manual investigation to find a better fit between the observed and the calculated $P_S(\theta)$. The single-scattering albedo of the model fits is included in Table 3, as well as the fine mode fraction of the aerosol optical thickness, calculated from the Mie extinction cross sections.

In Fig. 9(a) the lookup table fit (the Cabauw case) to the measurements of the degree of linear polarization as a function of viewing zenith angle is shown as a solid line. The mean deviation between the measurement and the simulation is 1.49%, and the root-mean-square error (RMSE) is 1.35%. The model parameters of this fit are shown in Table 3. Furthermore, a pure Rayleigh simulation (no aerosol) is shown to point out the influence of the added aerosol. Two simulations using aerosol microphysical parameters according to the AERONET climatology for Greenbelt, USA, and Paris, France, are also shown.[38] The aerosol microphysical parameters of the Greenbelt and Paris climatology are shown in Table 1. The decrease of polarization between the no-aerosol and aerosol-loaded

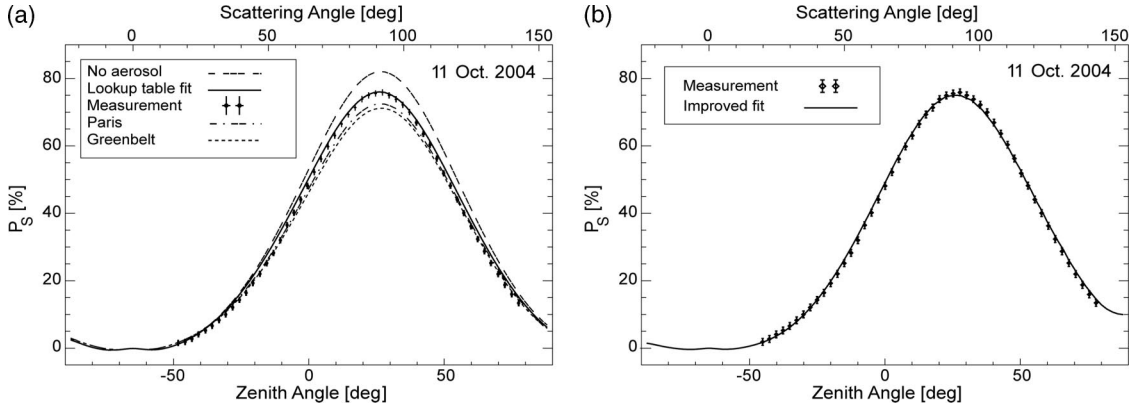

Fig. 9. Degree of linear polarization P_s at $\lambda = 675$ nm as a function of the viewing zenith and scattering angles in the principal plane at a solar zenith angle of $\theta_0 = 65°$, as measured on 11 October 2004 at Cabauw, The Netherlands. (a) Comparison with multiple scattering calculations for a pure molecular atmosphere (maximum of $P_s = 82.2\%$ at $\theta = 25°$), as well as for aerosol loaded atmospheres. All the input parameters are shown in Tables 1 and 2. The best fit between measurement and model result is indicated by a solid curve. (b) Comparison with an improved model fit (see Table 3).

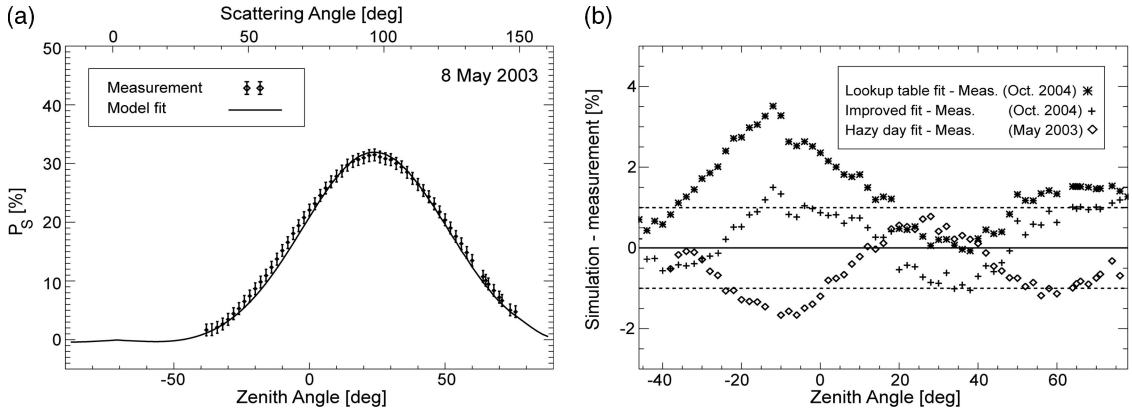

Fig. 10. (a) Degree of linear polarization P_s at $\lambda = 675$ nm as a function of the zenith and scattering angles in the principal plane at a solar zenith angle of $\theta_0 = 71°$ as measured on 8 May 2003 at Cabauw, The Netherlands, compared with the best fit. For the pure molecular atmosphere we derive a maximum of $P_s = 81.1\%$ at $\theta = 19°$. (b) Deviation between the measurement and the model fits. Dotted lines indicate a deviation of 1%.

simulations is attributable to scattering by aerosols, which gives a lower $P_s(\theta)$ than scattering by molecules (see Subsection 3.B). A shift in the position of the maximum degree of polarization takes place as well. The decrease is seen mainly in the backscattering direction and in the maximum degree of polarization. The simulations using the Greenbelt and the Paris aerosol microphysical parameters have a lower maximum degree of polarization than those with the lookup table fit.

The lookup table fit could be improved by varying the imaginary part of the refractive index, the weighting factor of the fine mode, and the standard deviation of the fine and coarse modes [see Fig. 9(b)]. After the improvement, the mean deviation between simulation and measurement is only 0.30% and the RMSE is reduced to 0.76%. The aerosol microphysical parameters of this improved fit are also shown in Table 3. The absolute deviation of $P_s(\theta)$ between the measurements and the model fit is shown in Fig. 10(b). Compared with the measurement, both model fits have a higher degree of linear polarization in the forward- and backscattering directions and a lower maximum degree of polarization. Given the fact that the measurement accuracy is 1%, the deviation is acceptable.

The effect on polarization because of the ozone absorption in the Chappuis band had been taken into account. The difference in the degree of polarization with and without ozone absorption is approximately -0.17% and affects mainly the backscattering direction.

As an indication of whether the aerosol size parameters were oriented in the right direction, we looked at the wavelength behavior of the maximum degree of polarization. The maximum degree of polarization at 675 nm was higher than at 465 nm (see Fig. 8). This is an indication of small particles.[49] Further, we looked at the Angström coefficient α. From the sun-photometer measurements we derived an α of 1.1 between 550 and 675 nm and of 2.3 between 675 and 780 nm. From the Mie extinction cross sections we calculated an α of 1.7 between 550 and 675 nm and of 2.5 between 675 and 780 nm. Thus the sun photometer measurements also indicated the presence of small particles, which strengthens the conclusion of the presence of small particles as found by the polarization measurements.

B. Hazy-Sky Comparison for 8 May 2003

Because of a higher aerosol optical thickness τ_{aer} and a higher surface albedo A, and because of a larger solar zenith angle θ_0 on the hazy day, we already expected a lower degree of linear polarization, compared with the measurements of the clear day. The increase of τ_{aer} resulted in an increase of the radiance and a decrease of $P_s(\theta)$. This is the result of more aerosol scatterers and hence more scattering in the line of sight by the less polarizing aerosols, compared with the molecules. The larger A decreases $P_s(\theta)$ because of an increase of depolarized light from the surface, whereas the larger θ_0 causes a shift in the position of the maximum degree of linear polarization to lower viewing zenith angles and a decrease of the effect of A (weaker illumination of the surface). As we have already seen in Section 3 we do not expect any influence on $P_s(\theta)$ because of the aerosol altitude. The comparison with the measurements of the clear day shows the expected shift of the position of the maximum to lower viewing zenith angles and a much lower degree of linear polarization [see Figs. 9(a), 9(b), and 10(a)]. Furthermore, we assume the presence of hygroscopic aerosols at the measurement site in Cabauw. With increasing relative humidity, it is generally expected that hygroscopic particles get larger and that the real and imaginary parts of the refractive index decrease. The relative humidity during the measurements was approximately 100%, compared to 81% on the clear day. Taking the microphysical parameters of the clear day as a starting point for the investigation, we increased the fine mode standard deviation and the median radii of the fine and coarse modes, whereas we decreased the real and imaginary parts of the refractive index, as well as

the weighting factor of the fine mode. In Fig. 10(a) the best fit to the FUBISS–POLAR measurements of the degree of linear polarization as a function of the viewing zenith angle in the principal plane is shown by a solid curve. The mean deviation between measurements and simulations is −0.81%, and the RMSE is 0.91%. The model parameters for this fit are shown in Table 3. The absolute difference of $P_s(\theta)$ between the model fit and the measurement is shown in Fig. 10(b). The model fit has a higher degree of polarization at approximately the maximum and a lower degree of polarization in the forward-scattering and backscattering directions. The difference between the measurements and the model for the hazy day is similar in magnitude and shape to that of the clear day, but reversed in sign. The reason for this is not clear because the difference is mostly below 1%, which is within the limits of measurement accuracy. The difference in the degree of polarization with and without ozone absorption in the Chappuis band is approximately −0.11%, and also affects mainly the backscattering direction.

As an indication of whether the aerosol size parameters are oriented in the right direction, we reexamined the wavelength behavior of the maximum degree of polarization. For this day we find a lower maximum degree of polarization at 675 nm than at 465 nm (see Fig. 8), which is an indication of larger particles.[49] The Angström coefficient α, derived from the sunphotometer measurements, is 0.5 between 550 and 675 nm and 0.8 between 675 and 780 nm. From the Mie extinction cross sections we calculated an α of 0.7 between 550 and 675 nm and of 0.9 between 675 and 780 nm. Thus the sunphotometer measurements also indicated the presence of larger particles on the hazy day than on the clear day.

6. Summary and Conclusions

The analysis of the dependence of the degree of linear polarization of skylight in the Sun's principal plane as a function of aerosol microphysical parameters using Mie calculations and multiple-scattering simulations shows that for a clear sky the degree of polarization is strongly influenced by the parameters of the fine mode of the aerosol size distribution (the median radius and geometric standard deviation), the real part of the aerosol refractive index, and the aerosol optical thickness. The other aerosol parameters show less influence. The sensitivity study was extended to hazy-sky conditions, where we found an increase of the sensitivity for the real and imaginary parts of the refractive index, whereas the sensitivity attributable to changes in the weighting factor of the fine mode decreases strongly. The strong influence of the fine mode parameters as well as of the aerosol optical thickness remains. The determination of some parameters, such as the imaginary parts of the refractive index, is complicated by the fact that we can have nonunique solutions. We find similar results for a different combination of aerosol parameters, for instance, by lowering the imaginary part and increasing the weighting factor, or the other way around. However, this results in two strongly differing single-scattering albedos. An accurate determination of the imaginary part of the refractive index does not seem to be possible if only polarimetry is used.

From this sensitivity study in the continuum (outside the absorption bands) we conclude that the number of free input parameters for the polarization radiative transfer simulations can be reduced from ten to seven (see Table 3), namely, the real and imaginary parts of the refractive index, the median radius and the geometric standard deviation of the fine mode, the aerosol optical thickness, the weighting factor of the fine mode, and the surface albedo. The parameters of the coarse mode of the size distribution and the aerosol altitude can be regarded as nonfree parameters, because of their minor influence on skylight polarization. The aerosol optical thickness should be measured together with the polarization of skylight because of the strong influence of the aerosol optical thickness and to further reduce the number of free input parameters.

From skylight polarization measurements in Cabauw, The Netherlands, we derived microphysical aerosol parameters by comparing the calculated degree of polarization with the measured degree of polarization. The best fit was found manually, by adjusting every input parameter until we found the best comparison between measurement and simulation. To avoid local minima problems, we took the whole zenith angle range into account for the comparison. Furthermore, we calculated the fine mode fraction of the aerosol optical thickness from the microphysical aerosol parameters derived from the comparison. The measurements were taken at clear- and hazy-sky conditions with FUBISS–POLAR, a ground-based multispectral and multiangle polarization spectrometer. The aerosol optical thickness was measured with a sunphotometer. The comparison of the measurements and simulations of the degree of linear polarization shows very good agreement. For the comparison we used a bimodal lognormal aerosol size distribution because simulations with a single-mode approach showed that it was not possible to match the position of the maximum degree of polarization of the measurements while finding an agreement in the forward-scattering and backscattering directions. As a measure of the quality of the solution we took the mean deviation and the RMSE. The difference between the model fits and the measurements of polarization was within the range of a measurement accuracy of 1% in degree of polarization. The RMSE between the model fit and the measured data was less than 0.92% for both test days. The model fit of the clear day seemed to overestimate the polarization measurements in the forward-scattering direction as well as in the backscattering direction, and underestimate it around the maximum degree of polarization. The model fit of the hazy day looks nearly mirror inverted to the clear-day model fit. The very good agreement between measurements and the simulations suggests that the basic assumption of Mie theory is applicable for the cases chosen here. If the sphericity as-

sumption would not have been applicable it would not have been possible to achieve a satisfactory fit to the polarization measurements.[12] Furthermore, we see that the resulting size distribution, derived from the comparison between the polarization measurements and the simulations tended to be in the same direction as suggested by the sunphotometer measurements and the investigation of the wavelength dependence measurements of the maximum degree of linear polarization.

From the sensitivity study and the comparison between the simulations and the measurements, we find that it is not sufficient to measure and/or simulate the degree of linear polarization only at a single-scattering angle in the principal plane, e.g., 90°. To estimate the aerosol properties reliably one has to find an agreement between the simulation and the measurement of polarization in the forward-scattering direction, in the backscattering direction, and the maximum, as was done here.

Based on this polarization study and previous studies[12,15,17,50] a retrieval algorithm will be developed to automatically retrieve aerosol microphysical and optical properties from skylight polarization measurements at multiple wavelengths.

Appendix A. Delta Approximation

The delta approximation consists of truncating the forward peak of F_{11} at a certain scattering angle Θ_c.[51] By doing so, the energy that is scattered in the near-forward directions is not considered to be scattered at all. Therefore the scattering cross section is reduced, and consequently the extinction cross section, the single-scattering albedo, and the optical thickness are changed. The truncated phase function has to be normalized. The truncation is done such that $F_{11}(\Theta) = F_{11}(\Theta_c)$ for $0 \le \Theta < \Theta_c$. The same is done for the other scattering matrix elements. The relative amount of energy that is truncated is

$$\delta = \int_0^{\theta_c} F_{11}(\Theta)\mathrm{d}\Omega - F_{11}(\Theta_c)\int_0^{\theta_c} \mathrm{d}\Omega. \tag{A1}$$

The scattering and extinction cross sections now reduce to

$$\sigma_s' = \sigma_s(1 - \delta), \tag{A2}$$

$$\sigma_e' = \sigma_e(1 - \delta\omega). \tag{A3}$$

The new single-scattering albedo is now

$$\omega' = \omega\,\frac{1 - \delta}{1 - \delta\omega}. \tag{A4}$$

The optical thickness is adjusted according to

$$\tau' = (1 - \delta\omega)\tau. \tag{A5}$$

The new phase function, together with the whole scattering matrix, is renormalized by

$$F_{11}'(\Theta) = \frac{1}{1 - \delta}\,F_{11}(\Theta). \tag{A6}$$

We acknowledge the support of the German Academic Exchange Service (DAAD) and the Royal Netherlands Meteorological Institute (KNMI) whose funding made part of the work reported here possible. We thank Oleg Dubovik for helpful suggestions on an earlier version of this paper.

References

1. J. T. Houghton, L. G. Meira Filho, B. A. Callander, N. Harris, A. Kattenberg, and K. Maskell, eds., *The Science of Climate Change* (Cambridge U. Press, 1995), pp. 1–572.
2. Y. J. Kaufman, D. Tanré, and O. Boucher, "A satellite view of aerosols in the climate system," Nature **419,** 215–223 (2002).
3. T. S. Ledley, E. T. Sundquist, S. E. Schwartz, D. K. Hall, J. D. Fellows, and T. L. Killeen, "Climate change and greenhouse gases," Eos Trans. Am. Geophys. Union **80,** 453–458 (1999).
4. J. T. Houghton, Y. Ding, D. J. Griggs, M. Noguer, P. J. van der Linden, X. Dai, K. Maskell, and C. A. Johnson, eds., "Climate Change 2001: the Scientific Basis" (Cambridge U. Press, 2001).
5. U. Lohmann and G. Lesins, "Stronger constraints on the anthropogenic indirect aerosol effect," Science **298,** 1012–1016 (2002).
6. R. J. Charlson, S. E. Schwartz, J. M. Hales, R. D. Cess, J. E. Coakley, J. E. Hansen, and J. D. Hofmann, "Climate forcing by anthropogenic aerosols," Science **255,** 423–430 (1992).
7. J.-L. Brenguier, H. Pawlowska, and L. Schueller, "Cloud microphysical and radiative properties for parameterization and satellite monitoring of the indirect effect of aerosol on climate," J. Geophys. Res. **108**(D15), 8632, doi:10.1029/2002JD002682 (2003).
8. J.-L. Brenguier, H. Pawlowska, L. Schueller, R. Preusker, J. Fischer, and Y. Fouquart, "Radiative properties of boundary layer clouds: droplet effective radius versus droplet concentration," J. Atmos. Sci. **57,** 803–821 (2000).
9. S. A. Twomey, M. Piepgrass, and T. L. Wolfe, "An assessment of the impact of pollution on global cloud albedo," Tellus Ser. B **36,** 356–366 (1984).
10. D. Rosenfeld and G. Feingold, "Explanation of discrepancies among satellite observations of the aerosol indirect effects," Geophys. Res. Lett. **30,** 1776, doi:10.1029/2003GL017684 (2003).
11. A. A. Lacis and M. I. Mishchenko, "Climate forcing, climate sensitivity, and climate response: A radiative modelling perspective on atmospheric aerosols" in *Aerosol Forcing of Climate,* R. J. Charlson and J. Heintzenberg, eds. (Wiley, 1995).
12. O. Dubovik and M. D. King, "A flexible inversion algorithm for retrieval of aerosol optical properties from Sun and sky radiance measurements," J. Geophys. Res. **105,** 20673–20696 (2000).
13. B. N. Holben, T. F. Eck, I. Slutsker, D. Tanré, J. P. Buis, A. Setzer, E. F. Vermote, J. A. Reagan, Y. J. Kaufman, T. Nakajima, F. Lavenu, I. Jankowiak, and A. Smirnov, "AERONET-A federated instrument network and data archive for aerosol characterization," Remote Sens. Environ. **66,** 1–16 (1998).
14. S. Mukai, I. Sano, and T. Takashima, "Investigation of atmospheric aerosols based on polarization measurements and scattering simulations," Opt. Rev. **3,** 487–491, 1996.
15. B. Cairns, B. E. Carlson, A. A. Lacis, and E. Russell, "An analysis of ground-based polarimetric sky radiance measurements," in *Proceedings of the Seventh Atmospheric Radiation*

Measurement (ARM) Science Meeting, ARM-CONF-1997 (San Antonio, Tex. 1997), pp. 51–57.
16. M. I. Mishchenko and L. D. Travis, "Satellite retrieval of aerosol properties over the ocean using measurements of reflected sunlight: Effect of instrumental errors and aerosol absorption," J. Geophys. Res. **102,** 13543–13553 (1997).
17. A. Vermeulen, C. Devaux, and M. Herman, "Retrieval of the scattering and microphysical properties of aerosols from ground-based optical measurements including polarization. I. Method," Appl. Opt. **39,** 6207–6220 (2000).
18. F. S. Zhao, Z. B. Gong, H. L. Hu, M. Tanaka, and T. Hayasaka, "Simultaneous determination of the aerosol complex index of refraction and size distribution from scattering measurements of polarized light," Appl. Opt. **36,** 7992–8001 (1997).
19. F.-M. Breon, J.-L. Deuzé, D. Tanre, and M. Herman, "Validation of spaceborne estimates of aerosol loading from sun photometer measurements with emphasis on polarization," J. Geophys. Res. **102,** 17187–17195 (1997).
20. B. Cairns, E. E. Russell, and L. D. Travis, "Research scanning polarimeter: calibration and ground-based measurements," in *Polarization: Measurement, Analysis, and Remote Sensing II,* D. H. Goldstein and D. B. Chenault, eds., Proc. SPIE **3754,** 186–196 (1999).
21. J. L. Deuzé, F. M. Bréon, P. Y. Deschamps, C. Devaux, and M. Herman, "Analysis of the POLDER (POLarization and Directionality of Earth's Reflectances) airborne instrument observations over land surfaces," Remote Sens. Environ. **45,** 137–154 (1993).
22. F. M. Schulz, K. Stamnes, and J. J. Stamnes, "Modeling the radiative transfer properties of media containing particles of moderately and highly elongated shape," Geophys. Res. Lett. **25,** 4481–4484 (1998).
23. K. Chamaillard, S. G. Jennings, C. Kleefeld, D. Ceburnis, and Y. J. Yoon, "Light backscattering and scattering by nonspherical sea-salt aerosols," J. Quant. Spectrosc. Radiat. Transfer **79-80,** 577–597 (2003).
24. M. I. Mishchenko, A. A. Lacis, B. E. Carlson, and L. D. Travis, "Nonsphericity of dustlike tropospheric aerosols: implications for aerosol remote sensing and climate modeling," Geophys. Res. Lett. **22,** 1077–1080 (1995).
25. R. A. Kahn, P. Banerjee, D. McDonald, and D. J. Diner, "Sensitivity of multiangle imaging to aerosol optical depth and to pure-particle size distribution and composition over ocean," J. Geophys. Res. **103,** 32195–32238 (1998).
26. F. Barnaba and G. P. Gobbi, "Lidar estimation of tropospheric aerosol extinction, surface area, and volume: maritime and desert-dust cases," J. Geophys. Res. **106,** 3005–3018 (2001).
27. T. Ruhtz, E. Boesche, and J. Fischer, "Development of a new sensor module for hyperspectral polarimetric measurements," in *Polarization Analysis and Measurement IV,* D. H. Goldstein, D. B. Chenault, W. G. Egan, and M. J. Duggin, eds., Proc. SPIE **4481,** 242–246 (2002).
28. S. Chandrasekhar, *Radiative Transfer* (Dover, 1960).
29. H. C. van de Hulst, *Light Scattering by Small Particles* (Dover, 1981).
30. W. A. Shurcliff, *Polarized Light* (Harvard U. Press, 1962).
31. J. W. Hovenier, C. Van der Mee, and H. Domke, *Transfer of Polarized Light in Planetary Atmospheres* (Kluwer, 2004).
32. P. Stammes, "Light scattering properties of aerosol and the radiation inside a planetary atmosphere," Ph.D. dissertation (Free University of Amsterdam, 1989).
33. W. G. Egan, "Polarization in remote sensing" in *Polarization and Remote Sensing,* W. G. Egan, ed., Proc. SPIE **1747,** 2–48 (1992).
34. K. N. Liou, *An Introduction to Atmospheric Radiation,* 2nd ed., Vol. 84 of International Geophysics Series (Academic, 2002).
35. W. A. de Rooij and C. C. A. H. van der Stap, "Expansion of Mie scattering matrices in generalized spherical functions," Astron. Astrophys. **131,** 237–248 (1984).
36. J. H. Seinfeld and S. N. Pandis, *Atmospheric Chemistry and Physics* (Wiley, 1997).
37. O. Torres, R. Decae, J. P. Veefkind, and G. de Leeuw, "OMI aerosol retrieval algorithm," in *OMI Algorithm Theoretical Basis Document, Volume III, Clouds, Aerosols, and Surface UV Irradiance,* P. Stammes, ed., NASA Goddard Space Flight Center, 1 August 2002, http://eospso.gsfc.nasa.gov/eos_homepage/for_scientists/atbd/.
38. O. Dubovik, B. Holben, T. F. Eck, A. Smirnov, Y. J. Kaufman, M. D. King, D. Tanré, and I. Slutsker, "Variability of Absorption and Optical Properties of Key Aerosol Types Observed in Worldwide Locations," J. Atmos. Sci. **59,** 590–608 (2001).
39. G. A. d'Almeida, P. Koepke, and E. P. Shettle, eds. *Atmospheric Aerosols–Global Climatology and Radiative Characteristics,* (Deepak, 1991).
40. J. W. de Haan, "Effects of aerosols on the brightness and polarization of cloudless planetary atmospheres," Ph.D. dissertation (Free University of Amsterdam, 1987).
41. P. Stammes, "Spectral radiance modelling in the UV-visible range," in *IRS 2000: Current problems in Atmospheric Radiation,* W. L. Smith and Y. M. Timofeyev, eds. (Deepak, 2001) pp. 385–388.
42. R. B. A. Koelemeijer, J. F. de Haan, and P. Stammes, "A database of spectral surface reflectivity in the range 335–772 nm derived from 5.5 years of GOME observations," J. Geophys. Res. **108**(D2), 4070, doi:10.1029/2002JD002429 (2003).
43. E. Boesche, "Aufbau und Beschreibung eines Polarisations-Spektrometers fuer die Fernerkundung der Atmosphaere," in *Radiation in Atmosphere and Ocean,* Book 23, J. Fischer, ed. (Institute for Space Sciences, Free University of Berlin, 2003).
44. B. Fitch and K. L. Couslon, "Polarizing radiometer measurements of skylight at South Pole Station, Antarctica," in *Optical Polarimetry: Instrumentation and Applications,* R. M. A. Azzam and D. L. Coffeen, eds., Proc. SPIE **112,** 184–190 (1977).
45. D. Beaglehole and G. G. Carter, "Antarctic skies 2. Characterization of the intensity and polarization of skylight in a high albedo environment," J. Geophys. Res. **97,** 2597–2600 (1992).
46. T. Takashima, K. Masuda, S. Mukai, and I. Sano, "Detection of atmospheric aerosol over Lunar Lake, Nevada, using ground-based skylight polarization measurements," Adv. Space Res. **23,** 1525–1528 (1999).
47. R. Preusker, U. Böttger, and J. Fischer, "Spectral and bidirectional measurements of the Stokes vector in the O_2A band and their interpretation," in *Atmospheric Sensing and Modeling II,* R. P. Santer, ed., Proc. SPIE **2582,** 13–20 (1995).
48. P. Stammes and J. S. Henzing, "Multispectral aerosol optical thickness at De Bilt, 1997–1999," J. Aerosol Sci. **31,** 283–284, special issue EAC 2000 (2000).
49. I. Aben, F. Helderman, and P. Stammes, "Spectral fine-structure in the polarization of skylight," Geophys. Res. Lett. **26,** 591–594 (1999).
50. O. Dubovik, "Optimization of numerical inversion in photopolarimetric remote sensing," in *Photopolarimetry in Remote Sensing,* G. Videen, Y. Yatskiv, and M. Mishchenko, eds. (Kluwer, 2004), pp. 65–106.
51. J. H. Joseph, W. J. Wiscombe, and J. A. Weinman, "The Delta–Eddington approximation for radiative flux transfer," J. Atmos. Sci. **33,** 2452–2459 (1976).